Research Article

Chemical Synthesis and Properties of Novel Bi_2Se_3 Nanostructures and Microplatelets

Cosmas M. Muiva,[1,2] Charles Moditswe,[1] and T. Stephen Sathiaraj[1]

[1] *Department of Physics, University of Botswana, Private Bag UB 0022 Gaborone, Botswana*
[2] *African Materials Science and Engineering Network (AMSEN), A Carnegie IAS-RISE Network,*
  UB Node, Private Bag UB 0022 Gaborone, Botswana

Correspondence should be addressed to Cosmas M. Muiva, cmuiva@yahoo.co.uk

Bi_2Se_3 nanostructures, microsised fibre bundles, and platelets have been synthesised through a simple chemical spray pyrolysis route on glass substrates. Low substrate temperatures (T_{sub}) favoured growth of nanostructures while elevated T_{sub} was accompanied by increased grain growth and formation of microsised platelets. The nanostructures were identified as nanorods, nanofibers, nanotubes, nanoflowers, and nanoneedles of various aspect ratios. There was an observed red shift of the optical band gap (E_g^{opt}) with increased T_{sub} from 2.40 eV at 95°C to 1.25 eV at 360°C. Thermo probe measurements confirmed n-type conductivity with dark resistivities which followed a near exponential decline with elevated T_{sub}. The observed changes in optoelectronic properties existing in the different T_{sub} regimes were explained on the basis of microstructural and textural changes in the pristine clusters.

1. Introduction

Recently, research attention geared toward chemical and electrochemical synthesis of nanostructured colloidal chalcogenide semiconductors has increased several folds [1–10]. In this group, Bi_2Se_3 nano- and microsised clusters, isolated or well-adhered morphological orientations have been reported in literature. Ota et al. [1] has described synthesis and characterization of Bi_2Se_3 nanorods through a hydrothermal method. Nearly spherical grains by chemical bath deposition (CBD) were reported recently by Bari and Patil [2]. Other reports include hexagonal rod like nanostructures by convectional solvothermal method [3] and microplatelets by single-source precursor metal-organic chemical vapour deposition (MOCVD) [4]. A number of interesting nanostructures such as hexagonal nanosheets and nanotubes through hydrothermal coreduction [5] and hexagonal nanoflakes through a novel solvothermal method [6] were recently fabricated and characterised. In addition, nanocrystalline thin films by electrochemical atomic layer epitaxy (ECALE) [7] and successive ionic layer adsorption and reaction (SILAR) [8] were reported. Li et al. [9] have synthesised and traced shape evolution of novel bismuth selenide hollow nanospheres through precipitation in a capping agent while thermally evaporated structures have been discussed by Manjulavalli et al. [10].

Reduced dimensions and different shapes in the nanoregime are quite an attractive recipe for applications owing to reduced dimensions or surface area catalysis of the well-known properties. Beside applications such as photosensitive devices, Hall-effect magnetometer, high-frequency power sensor thermopiles, solar selective decorative coating, wide band radiation detectors, and humidity sensors using the Seebeck and Peltier effects, addition of a third element such as Te to Bi_2Se_3 is known to produce the best thermoelectric properties so far reported [11]. In this paper we report cheap synthesis and characterisation of Bi_2Se_3 nanostructures (nanorods, nanofibres, nanotubes, nanoflowers, and nanoneedles) and microplatelets grown on glass substrates through a simple chemical spray pyrolysis technique.
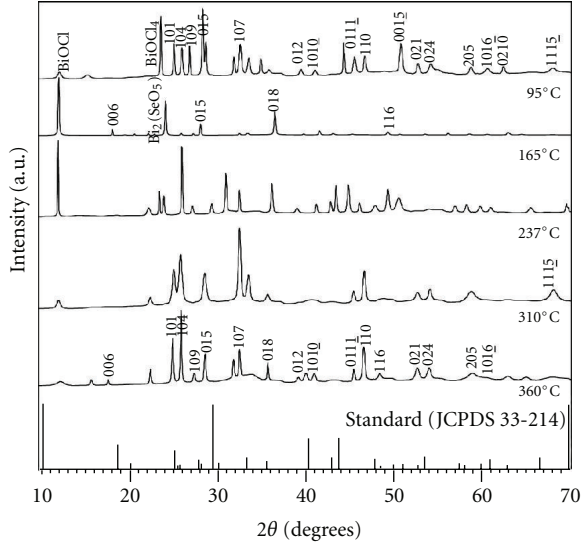
FIGURE 1: XRD diffractographs of Bi_2Se_3.

TABLE 1: Grain size (D) and dislocation density (δ) of Bi_2Se_3 nanostructures.

T_{sub} °C	Method	Particle (diameter)	D (nm)	δ $(nm)^{-2}$
95	SEM	Needles	96	0.00011
	SEM	Rods	102	0.00010
	SEM	Needles	68	0.00022
165	SEM	Tubes (inner)/needles	193/59	—
	SEM	Fibers	64	0.00024
	SEM	Fiber bundles	Undefined	—
	SEM	Flowers/needles	136/31	—

2. Experimental Details

Bi_2Se_3 nanostructures and microplatelets were prepared using a chemical spray pyrolysis set up described elsewhere [12, 13]. The starting analytical grade compounds were purchased from Sigma-Aldrich and used without further processing. The precursor solution was a mixture of 0.1 M selenourea ($SeC(NH_2)_2$) and 0.1 M bismuth (III) chloride ($BiCl_3$) dissolved in 85% acetone and 15% water. The solution was sprayed on 3 cm × 7 cm precleaned glass substrates held 12 cm below the spray nozzle. The spray rate for all the samples was 2 mL/min making a total of 30 mL for each spray cycle which lasted 15 min. A bimetallic thermometer that could measure the temperature to an accuracy of ±1°C was used to measure the substrate temperature (T_{sub}). A set of samples were deposited at each operating temperature (95°C, 165°C, 237°C, 310°C, and 360°C).

The crystallographic phases and structure of the material were examined with a Philips PW-3710 X-ray diffraction (XRD) system using Cu Kα radiation (λ = 1.5418 Å) operating at 40 kV, 30 mA. The surface morphology of the sample was studied using a Philips XL 30 scanning electron microscope (SEM) fitted with an energy dispersive spectroscopy (EDS) detector for elemental composition analysis. A double beam Cary 500 UV/VIS/NIR spectrophotometer was used for the optical characterisation of the clusters by collecting the incident transmittance (T) and reflectance (R) spectra in the spectral range 300–2500 nm. A Keithley-based four-point probe set-up was used to collect I-V data.

3. Results and Discussion

Figure 1 shows XRD diffractographs of Bi_2Se_3 structures prepared at different T_{sub}. The observed Bi_2Se_3 diffraction peaks correspond to hexagonal crystallographic lattice (JCPDS 33-0214) with space group: $R3m$ (166).

The XRD pattern shows that samples prepared at low T_{sub} are not of high purity because of too many reflections that cannot be indexed to a pure phase of Bi_2Se_3. Conspicuously, a sample prepared at 95°C reveal other crystallographic presentations which could not be assigned to Bi_2Se_3. These unidentified peaks were assigned to impurities and included $BiOCl$, $BiOCl_4$, and $Bi_2(SeO_5)$. An EDS scan confirmed presence of oxygen and chlorine in the samples prepared at 95°C and 165°C. At higher temperatures, both XRD and EDS showed presence of Bi_2Se_3 only. It is anticipated that owing to low temperature there was partial decomposition of the precursor leading to formation of some by products and undecomposed metalorganics. At higher temperature, there was complete decomposition of the precursor and vaporisation of the volatile by products. The oxygen may have formed SeO which sublimed at higher temperatures.

The dislocation density (δ) of the crystallites in the Bi_2Se_3 films at varied T_{sub} was obtained from (2) [14] while grain size (D) was calculated using the Deby-Scherrer's [15] formula

$$D = \frac{0.9\lambda}{\beta \cos\theta}, \tag{1}$$

$$\delta = mD^{-2}, \tag{2}$$

where λ is the wavelength of the X-rays used, β the full width at half maximum of the peak in radian, θ the Bragg's angle of diffraction, and m is usually a constant $\approx$ unity. The values of D and δ are shown in Table 1.

SEM images (Figure 2(a)) reveals nanoneedles embedded in an amorphous matrix. In the low T_{sub} regimes, nanoparticles of different morphologies and shapes are formed while the growth shifts towards microplatelets at higher substrate temperatures. The nanoparticles formed at 95°C (Figure 2(a)) are not well defined. They were identified as nanoneedles with random orientations along all directions. This random orientation implies low adatom surface energies and lifetimes on the substrate surface.

At 165°C, the observed surface was too warped with dislocations and cavities. Nanoparticles of different shapes, sizes, aspect ratios, and morphologies were observed in different cavities of the same substrate. The distinct ones were identified as nanoneedles, nanofibers, nanorods, nanotubes, and microflowers. Although pure clusters of nanoneedles were observed in some cavities, SEM images reveal that these microflowers and nanotubes are build up through
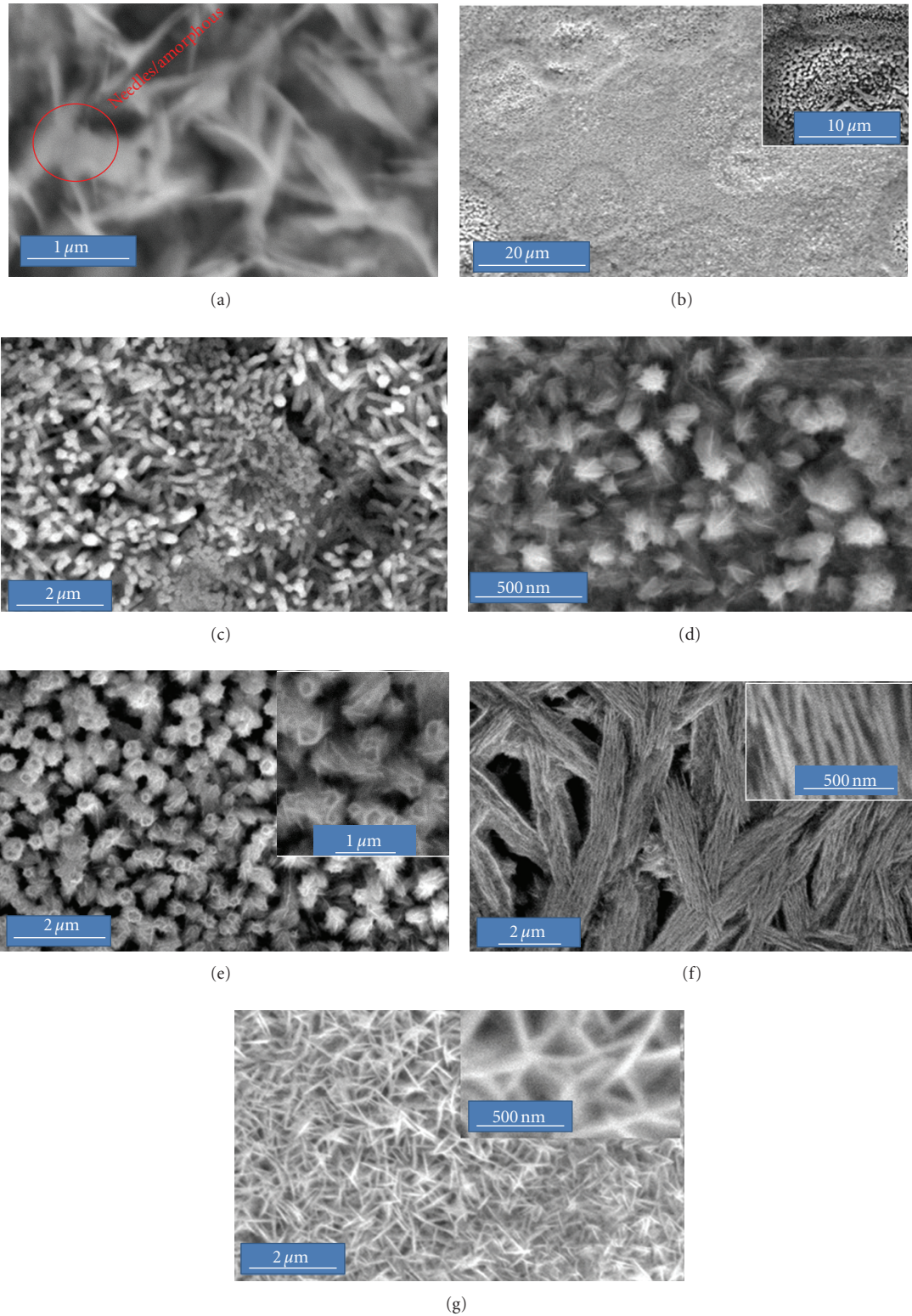
FIGURE 2: (a) Bi$_2$Se$_3$ nanostructures formed at a T_{sub} of 95°C. (b–g): SEM images of Bi$_2$Se$_3$ nanostructures synthesised at a T_{sub} of 165°C. Nanoparticle laden warping and cavities (b), nanorods (c), nanoflowers (d), hollow nanotubes (e), nanofibers (f), and nanoneedles (g). Insets are the close up images.
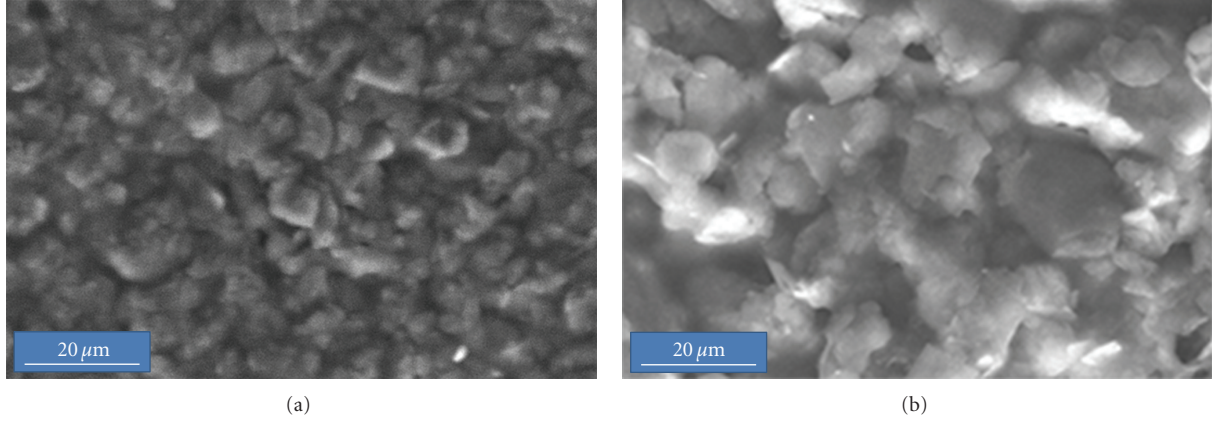
(a)

(b)

FIGURE 3: SEM images of Bi_2Se_3 microplatelets of a sample synthesized at a T_{sub} of 310°C (a) and 360°C (b).

TABLE 2: Lattice parameters of Bi_2Se_3 clusters from 101 and 107 diffraction planes (310°C).

	Bi_2Se_3					
	a (Å)	c (Å)	V (Å)^3	$l = c/a$	a_R	$\alpha°$
Standard lattice parameters [JCPDS 33-214]	4.1396	28.6360	423.2	6.9176	9.840	24.878
Calculated lattice parameters	4.2917	29.3918	434.6	7.0918	10.106	25.130
% deviation	3.6740	2.6390	2.6	2.5	2.7	1.0

aggregation of nanoneedles in regular patterns. Similarly, the nanofibers clung together to form bundles of irregular lengths and widths. The aspect ratio of the nanoneedles (l/w), Figure 2(g), was found to be in the range of 14.2. The cavities may be due to gases evaporating coupled with lack of enough thermal energy for reorganisation due to low lifetime of adatoms. The difference shapes, sizes, and morphologies may be due to thermal gradients along the substrate which was possibly the optimum temperature for nanoparticle formation. At these low T_{sub}, the slowly evaporating solvent may have acted as a capping agent leading to formation of isolated nanoparticles. The observed nanoparticles were oriented length wise parallel to the substrate surface. The grain sizes (D) were also estimated by random sampling and averaging from SEM images. The values were entered in Table 1.

SEM images (Figures 3(a) and 3(b)) reveal that at 310°C and 360°C, growth shifted towards irregularly shaped microplatelets with cross-sectional spans of up to 10 μm. There was enhanced increase in size as the T_{sub} changed from 310°C to 360°C. High surface energy indicates high adatom mobility and increased lifetime on the substrate surface [16]. It can therefore be concluded that nuclei yielding platelets represent the lowest surface energy. The same microplatelets were observed by others [4] using single source MOCVD at precursor temperature of 275°C and T_{sub} of 425°C.

The lattice parameters were calculated using the expression [10, 17]

$$\frac{1}{d} = \left(\frac{4}{3}\right)\left[\frac{(h^2 + hk + k^2)}{a^2}\right] + \left(\frac{l^2}{c^2}\right), \tag{3}$$

where h, k, and l are the miller indices of the crystallographic planes, a and c are the lattice parameters, and $l = c/a$

is the lattice constant. For hexagonal structure the lattice parameters a and c are related to the lattice angles a_R and $\alpha°$ through [18, 19]

$$a_R = \frac{1}{3(3a^2 + c^2)^{1/2}},$$

$$\sin \alpha^2 = 3\left[\frac{1}{\left(3 + (c/a)^2\right)^{1/2}}\right]. \tag{4}$$

The observed values of a, c, l, a_R, and $\alpha°$ are shown in Table 2. The values have been compared to standard values of Bi_2Se_3. The calculated values are corresponding to standard values of hexagonal Bi_2Se_3 confirming that the samples are hexagonal Bi_2Se_3. The deviation of the experimental cell parameters and angles from the cell parameters in JCPDS 33-214 may be due to strain in the material resulting to elongated bonds and consequently higher cell parameters (a and c) [10].

The percentage of incident radiation transmitted through the samples was determined from spectrophotometric measurements and presented in Figure 4. An absorption edge corresponding to the spectral wavelengths (λ), 480–750 nm, was observed. Interference fridges observed for Bi_2Se_3 prepared at 95°C in the NIR region was explained on the basis of the difference in the refractive index of the smoother sample and substrate. There was no outright absorption edge and the observed curves were seen to rise gradually which may have been due to impurities and mixed clusters each presenting a distinct absorption edge. The recorded transmission of a sample fabricated at 165°C was low due to small grains, rough surface, and higher dislocation densities, all contributing elevated scattering of photons.

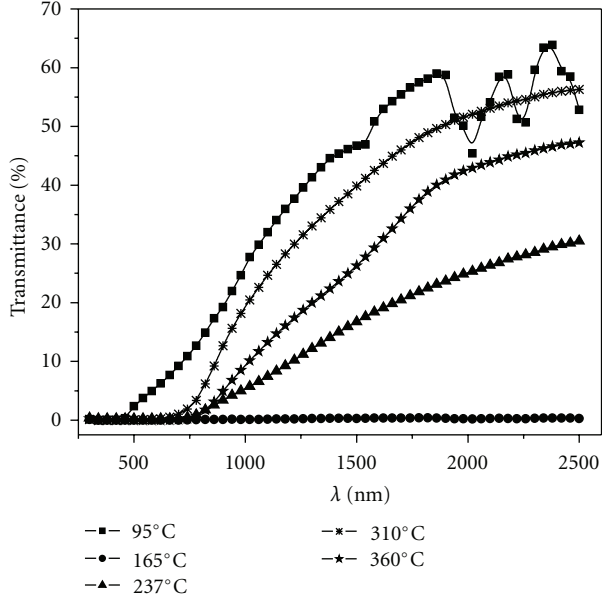FIGURE 4: Transmittance spectra of Bi_2Se_3 prepared at different T_{sub}.

The optical absorption coefficient α is determined from transmittance spectra T and film thickness t using the relation:

$$\alpha = \left(\frac{1}{t}\right)\ln\left(\frac{1}{T}\right). \qquad (5)$$

The optical absorption is related to the incident photon energy $(h\nu)$ by the following equation [20]

$$\alpha h\nu = B\left(h\nu - E_g\right)^n, \qquad (6)$$

where E_g is the optical band gap, ν the frequency of the photons, B is a constant referred to as the band tailing parameter, and n can take values 1/2, 3/2, 2, and 3 depending on the mechanism of transition across the energy gap. From the obtained plots, $n = 1/2$ offers the best fit which is consistent with allowed direct transitions. The value of E_g can be obtained by plotting $(\alpha h\nu)^2$ versus $h\nu$ as shown in Figure 5.

The observed plots have a linear portion from where E_g can be obtained by extrapolation towards $\alpha \rightarrow 0$. In this region, the absorption coefficient is of the order of $>10^4\,cm^{-1}$. The observed values of E_g are shown as an inset in Figure 5 and the range is consistent with those reported earlier through other deposition methods 2.25 eV [1], 1.5 eV [3], 2.35 eV [14], and 1.7–1.41 eV [21]. There was a red shift towards lower energies with increasing substrate temperature for the samples. Lower values have been reported in thin films, 0.35 eV [7] and 0.55 eV [22]. This wider band gap values in nanostructures may be due to quantum confinement effects [1]. For our case the largest band gap value 2.40 eV was observed for the lowest T_{sub} of 95°C. We observed a similar widening of the band gap at lower T_{sub} in spray-pyrolysed In_2Se_3 [23] thin films, which was attributed to presence of impurities such as oxides which are known to have wide band gap values. Presence of these
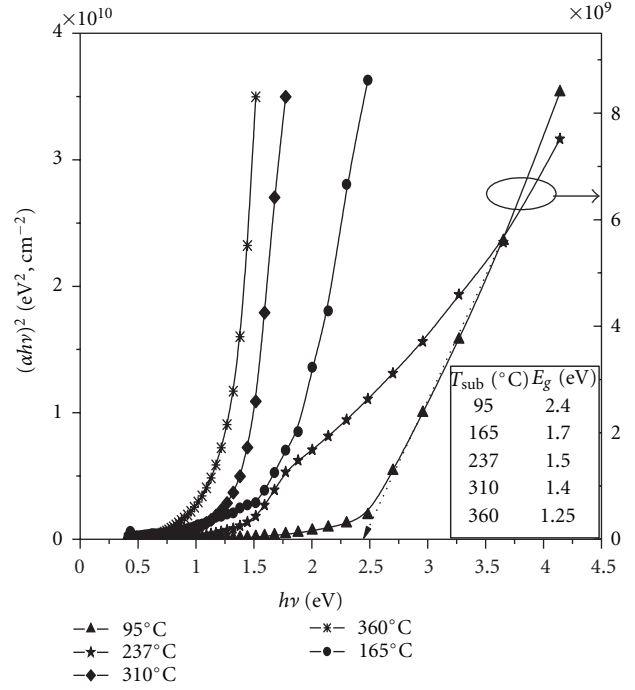

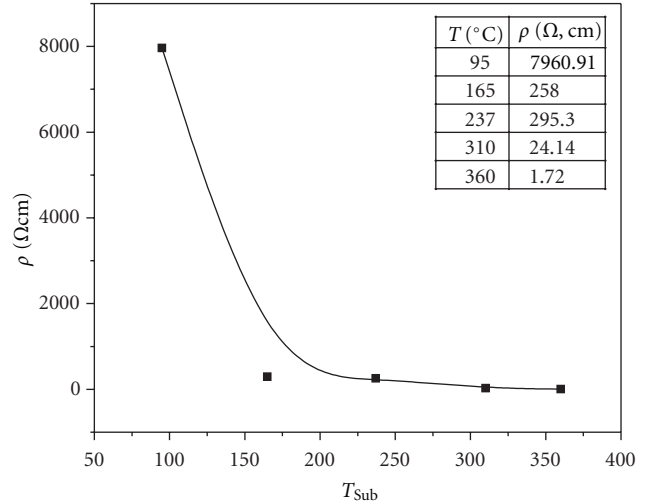FIGURE 5: Plot of $(\alpha h\nu)^2$ and photon energy $h\nu$ for Bi_2Se_3 prepared at different T_{sub}.

FIGURE 6: Variation of electrical resistivity of Bi_2Se_3 as a function of temperature.

impurities in the present case was detected during both XRD and EDS analysis.

Thermo probe studies established that all the samples synthesized in this study showed n-type dark conductivity. The resistivity (ρ) values were calculated from the I-V characteristics measured at room temperature (300 K) from the expression $\rho = (\pi/\ln 2)(V/I)t$, where t is the film thickness and V/I is the slope of a V against I plot. Sampling and averaging techniques were used since the clusters prepared at 165°C were inhomogeneous. The resistivity values as a function of T_{sub} are shown in Figure 6. The resistivity curve

displayed a monotonic decline (Figure 6) with T_{sub} from an order of $10^3\,\Omega\,\text{cm}$ at $95°C$ to $10^0\,\Omega\,\text{cm}$ at $360°C$. Improved conductivity was attributed to better crystallinity with increased substrate temperature resulting from better stacking of the film. It is anticipated that at lower temperature the adatoms are having very low surface energies and their mobility over the substrate is very low with consequent random stacking of the grains resulting in high porosity [16]. Moreover, at these low T_{sub} volatile by products which would have been vaporised at higher temperatures get trapped in grain boundaries and pores acting as carrier traps or sources of potential barriers increasing the resistivity. Increased grain sizes at higher temperatures imply lower dislocation densities (Table 1) and hence lower densities of grain boundaries.
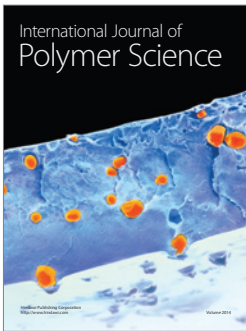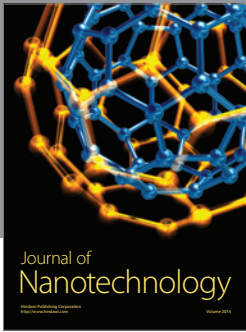
4. Conclusions

Nano- and microsised structures of Bi_2Se_3 thin films were prepared by CSPT. The optical band gap was observed to decrease with T_{sub} with a minimum value of 1.25 eV at $360°C$. The morphology of growth was influenced by the T_{sub} with low T_{sub} favouring growth of nanoparticles while high T_{sub} resulted to microplatelets. XRD studies confirmed formation of hexagonal Bi_2Se_3 with typical lattice parameters, $a = 4.2917\,\text{Å}$, $c = 29.3918\,\text{Å}$, and $c/a = 7.0918$ for a sample prepared at $310°C$. An n-type dark conductivity was observed for all the samples with resistivities that decreased with elevated T_{sub} and grain size.

Acknowledgments

References

[1] J. R. Ota, P. Roy, S. K. Srivastava, R. Popovitz-Biro, and R. Tenne, "A simple hydrothermal method for the growth of Bi_2Se_3 nanorods," *Nanotechnology*, vol. 17, no. 6, pp. 1700–1705, 2006.

[2] R. H. Bari and L. A. Patil, "Synthesis and characterization of bismuth selenide thin films by chemical bath deposition technique," *Indian Journal of Pure and Applied Physics*, vol. 48, no. 2, pp. 127–132, 2010.

[3] X. Yang, X. Wang, and Z. Zhang, "Synthesis and optical properties of single-crystalline bismuth selenide nanorods via a convenient route," *Journal of Crystal Growth*, vol. 276, no. 3-4, pp. 566–570, 2005.

[4] J. Waters, D. Crouch, P. O'Brien, and J. H. Park, "Fabrication of thin films of bismuth selenide using novel single-source precursors by metal organic chemical vapor deposition," *Journal of Materials Science*, vol. 14, no. 9, pp. 599–602, 2003.

[5] H. Cui, H. Liu, X. Li et al., "Synthesis of Bi_2Se_3 thermoelectric nanosheets and nanotubes through hydrothermal co-reduction method," *Journal of Solid State Chemistry*, vol. 177, no. 11, pp. 4001–4006, 2004.

[6] K. Kadel, L. Kumari, W. Z. Li, J. Y. Huang, and P. P. Provencio, "Synthesis and thermoelectric properties of Bi_2Se_3 nanostructures," *Nanoscale Research Letters*, vol. 6, no. 1, article 57, 2011.

[7] C. Xiao, J. Yang, W. Zhu, J. Peng, and J. Zhang, "Electrodeposition and characterization of Bi_2Se_3 thin films by electrochemical atomic layer epitaxy (ECALE)," *Electrochimica Acta*, vol. 54, no. 27, pp. 6821–6826, 2009.

[8] B. R. Sankapala and C. D. Lokhande, "Photoelectrochemical characterization of Bi2Se3 thin films deposited by SILAR technique," *Materials Chemistry and Physics*, vol. 73, p. 151, 2002.

[9] J. Li, Y. Zhu, J. Du, J. Zhang, and Y. Qian, "Synthesis and shape evolution of bismuth selenide hollow nanospheres," *Solid State Communications*, vol. 147, no. 1-2, pp. 36–40, 2008.

[10] T. E. Manjulavalli, T. Balasubramanian, and D. Nataraj, "Structural and optical properties of thermally evaporated Bi_2Se_3 thin film," *Chalcogenide Letters*, vol. 5, pp. 297–302, 2008.

[11] R. Venkatasubramanian, E. Siivola, T. Colpitts, and B. O'Quinn, "Thin-film thermoelectric devices with high room-temperature figures of merit," *Nature*, vol. 413, no. 6856, pp. 597–602, 2001.

[12] C. Muiva, S. T. Sathiaraj, and K. Maabong, "Chemical spray pyrolysis path to synthesis of ZnO microsausages from aggregation of elongated double tipped nanoparticles," *Materials Science Forum*, vol. 706–709, pp. 2577–2582, 2012.

[13] C. M. Muiva, T. S. Sathiaraj, and K. Maabong, "Effect of doping concentration on the properties of aluminium doped zinc oxide thin films prepared by spray pyrolysis for transparent electrode applications," *Ceramics International*, vol. 37, no. 2, pp. 555–560, 2011.

[14] S. Subramanian and D. P. Padiyan, "Effect of structural, electrical and optical properties of electrodeposited bismuth selenide thin films in polyaniline aqueous medium," *Materials Chemistry and Physics*, vol. 107, no. 2-3, pp. 392–398, 2008.

[15] D. Cullity and S. R. Stock, *Elements of X-Ray Diffraction*, Prentice-Hall, New York, USA, 3rd edition, 2001.

[16] A. van der Drift, "Evolutionary selection, a principle governing growth orientation in vapour-deposited layers," *Philips Research Reports*, vol. 22, pp. 267–288, 1967.

[17] B. E. Warren, *X-Ray Diffraction*, Dover, New York, NY, USA, 1990.

[18] Z. Abdel-Khalek Ali, G. H. Adel, and A. S. Abd-Rbo, "Structural and electrical properties of the chalcogenide glasses Bi30 Se(70-x) Tex system," *Chalcogenide Letters*, vol. 6, no. 6, pp. 265–271, 2009.

[19] V. Leonid, V. Azaroff, and M. J. Buerger, *The Powder Method in X-Ray Crystallography*, McGraw-Hill, New York, NY, USA, 1958.

[20] J. I. Pankove, *Optical Processes in Semiconductors*, Prentice-Hall, Englewood Cliffs, NJ, USA, 1971.

[21] V. M. García, M. T. S. Nair, P. K. Nair, and R. A. Zingaro, "Chemical deposition of bismuth selenide thin films using N,N-dimethylselenourea," *Semiconductor Science and Technology*, vol. 12, no. 5, pp. 645–653, 1997.

[22] A. P. Torane, C. D. Lokhande, P. S. Patil, and C. H. Bhosale, "Preparation and characterization of electrodeposited Bi_2Se_3 thin films," *Materials Chemistry and Physics*, vol. 55, no. 1, pp. 51–54, 1998.

[23] C. M. Muiva, S. T. Sathiaraj, and J. M. Mwabora, "Thermal and compositional defects in chemical spray pyrolysed indium selenide (In2Se3) thin films: effects on film properties," *Journal of Optoelectronics and Advanced Materials*, vol. 13, p. 1240, 2011.